Packing of nonoverlapping cubic particles: Computational algorithms and microstructural characteristics

Hessam Malmir and Muhammad Sahimi*
Mork Family Department of Chemical Engineering and Materials Science, University of Southern California, Los Angeles, California 90089-1211, USA

M. Reza Rahimi Tabar
Department of Physics, Sharif University of Technology, Tehran 11365-9161, Iran
(Received 31 August 2016; published 1 December 2016)

Packing of cubic particles arises in a variety of problems, ranging from biological materials to colloids and the fabrication of new types of porous materials with controlled morphology. The properties of such packings may also be relevant to problems involving suspensions of cubic zeolites, precipitation of salt crystals during CO_2 sequestration in rock, and intrusion of fresh water in aquifers by saline water. Not much is known, however, about the structure and statistical descriptors of such packings. We present a detailed simulation and microstructural characterization of packings of nonoverlapping monodisperse cubic particles, following up on our preliminary results [H. Malmir *et al.*, Sci. Rep. **6**, 35024 (2016)]. A modification of the random sequential addition (RSA) algorithm has been developed to generate such packings, and a variety of microstructural descriptors, including the radial distribution function, the face-normal correlation function, two-point probability and cluster functions, the lineal-path function, the pore-size distribution function, and surface-surface and surface-void correlation functions, have been computed, along with the specific surface and mean chord length of the packings. The results indicate the existence of both spatial and orientational long-range order as the the packing density increases. The maximum packing fraction achievable with the RSA method is about 0.57, which represents the limit for a structure similar to liquid crystals.

DOI: 10.1103/PhysRevE.94.062901

I. INTRODUCTION

Porous media and materials are of fundamental scientific and technological interest due to their wide variety of applications. The ability of porous media to interact with gases and liquids, not only on their external surface but also in their pore space as fluids pass through them, is one important factor in the wide interest in these materials. Other factors that contribute to the importance of porous media and materials include their capacity for storing energy (such as supercapacitors separating the components of a fluid mixture), their mechanical strength, and the thermal and electrical properties of their solid matrix. The structure of porous materials and media can be completely ordered [1] or stochastic with some degree of randomness or heterogeneity. Examples of ordered porous media include zeolites [2], which are used heavily in the chemical industry, and various types of aluminophosphates, which have a variety of applications. Disordered porous media may also be divided into two groups. One group consists of consolidated porous media in which the grains have somehow been fused together. Examples are too numerous, but they include rock, membranes, and other types of porous structures [3]. The second group is made up of unconsolidated porous media in the form of packing of nonoverlapping discrete particles. The focus of the present paper is on one particular type of packing.

The properties of packings of nonoverlapping particles have been studied intensively because, at the fundamental level, they are conceptual models for studying and understanding the structure of liquids, glassy and crystal states of matter [4-6], granular media [7], and heterogeneous materials [6,8,9]. As far as applications are concerned, packings of particles are relevant to powders [10], cell membranes [11], thin films [12], colloidal dispersion [13], and composite materials [6,8,9]. The great majority of early studies on packings of nonoverlapping particles focused on those with a spherical shape [6], with relatively limited studies of elliptical particles [14-19]. With the more recent widening range of applications of packings of particles, as well as advances in computational power and instrumentation, packings of other types of particles have also been studied, including disks [20,21], hard rectangles [22], polyhedra [23-26], tetrahedra [27-29], and other types [30,31].

Efficient computer generation of packings of particles is also a difficult problem. Thus, several algorithms for generating various types of packings have been developed. They include the random sequential addition (RSA) algorithm [15,32-36], particle-growth molecular dynamics (MD) [20,37-39], and Monte Carlo (MC) schemes [21,22,40,41]. Many of the issues relevant to packings of solid objects have been reviewed comprehensively by Torquato and Stillinger [42].

In this paper, we study the characterization of packings of cubic particles. The problem was motivated by a method of fabrication of porous materials developed recently by one of us (M.S.) and his collaborators [43]. Briefly, in this method, a salt (e.g., NaCl) that consists of cubic crystals and is suspended in a nonsoluble medium, such as alcohol or ketone, is used to coat a nonporous surface that can be, for example, plastic films, metal foils, or glass. A thermoplastic polymeric film, e.g.,

*moe@usc.edu

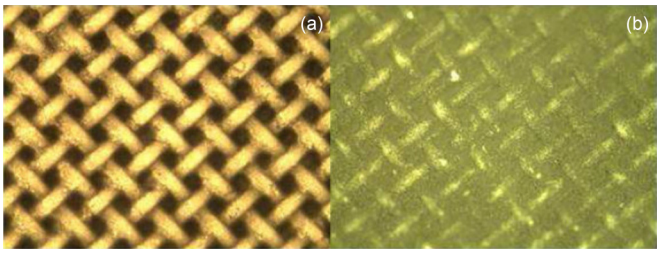

FIG. 1. (a) Salt suspension printed on a polyethylene terephthalate carrier. (b) Porous pattern formed by a cast vinyl film [43].

polyolefins or polyvinyl chloride (vinyl), is then hot-pressed over the salt layer. The polymeric material fills the void space between the salt crystals and solidifies upon cooling. The salt is then washed off with water. The voids created by removing the salt crystals create and expose the porous medium. Note that, as the melting temperature of most salt crystals is very high, they preserve their shapes and structure when the polymeric material is hot-pressed over the salt layer. The salt-coating process may be performed using various methods, and various porous patterns can be fabricated on a single surface. For example, a checkerboard porous pattern was created on vinyl using screen printing of a salt paste; see Fig. 1. In this case, not all of the surface was covered by the salt layer, rather a certain mesh pattern on it was covered. Note that, instead of salt, one can use other types of powders, as long as its particles do not melt during hot-pressing and can be easily washed off, and the thickness of the porous materials fabricated using this method can be established at the outset.

It is known [3] that, depending on the viscosity contrast between a fluid that invades a porous medium and the fluid (gas or liquid) that occupies the medium, a wide variety of patterns of displacements may be created, ranging from completely compact structures to highly branched and fractal-like patterns. Since in the context of the fabrication method that we are describing here the invaded portion of the packing constitutes the solid matrix of the eventual porous material after the invading fluid solidifies, one can fabricate porous materials with a wide variety of microstructures for various applications by using various fluids as the displacing and displaced agents [43]. It is for these reasons that the study of packings of cubic crystals is important.

The proposed fabrication method has many distinct advantages over practically all of the previous methods. (i) Since the porous medium is prepared by invading the salt packing, washing it off is easy, as all the crystals are accessible through their contact with each other. (ii) The pore-size distribution and pore connectivity of the porous sample are controlled completely by the size distribution of the salt crystals and their packing. The voids that are created by washing off the salt are the pores through which fluid flow and transport, as well as sorption, reaction, and mixture separation, occur in any particular application. Thus, the size distribution of the pores is *exactly the same as that of the salt crystals*, which can be measured *before* the porous medium is even fabricated. (iii) One has complete information on the pore space morphology. Therefore, one no longer needs to use such methods as mercury porosimetry in order to determine the pore-size distribution. Such methods either do not provide complete information, or they are limited to certain ranges of pore sizes. (iv) One can *design* any size distribution by selecting the appropriate crystal shapes and size distribution. Note that the size of the salt crystals can be controlled, so that the desired particle-size distribution is obtained. One method for doing so is recrystallization or precipitation, which is done by dissolving the salt in water. If we then add the solution to a nonsolvent (such as acetone), the salt begins to precipitate. By controlling the amount of the salt solution, the temperature and other thermodynamic factors, as well as the mixing conditions, we can obtain a wide range of sizes for the salt crystals. Further control of the particle size is achieved by either fractionation or sieving.

Since the pore space fabricated by the aforementioned method is *exactly* the same as the packing of the cubic salt crystals, the characterization of such a packing provides deep insight into the morphology of the pore space, and perhaps affords one even more control of the type and structure of the porous materials that are produced. In addition, packing of cubic particles is encountered in biological materials, colloids [44], and other types of systems of scientific importance. An important practical example is the evaporation of saline water. As evaporation proceeds, salt crystallizes and precipitates on the surface of the system in which the water is flowing, giving rise to a packing of cubic salt crystals that damages the surface. Understanding this phenomenon and how the packing changes the morphology of the system in which salt has precipitated, and hence its flow and transport properties, is of fundamental importance to the preservation of pavements, paintings, and historical monuments, mineral-fluid interactions, CO_2 sequestration in rock, and intrusion of groundwater aquifers by saline water, as the world faces increasing difficulty in obtaining drinking water [45].

The rest of the paper is organized as follows. In Sec. II, the RSA algorithm to generate the random packings of nonoverlapping equal-size cubic particles is presented. We also discuss the possibility of using other methods to generate random packings of cubes. Then, a variety of important statistical descriptors for the characterization of packings of cubic particles are described in Sec. III. The results are reported and discussed in Sec. IV. Section V summarizes the paper and discusses possible further research.

II. THE RSA ALGORITHM

We first note that various MD and MC methods that have been used for hard-particle packings are not applicable to the generation of packing of cubes, because the overlap potential functions cannot be constructed for particles with nonsmooth shapes including all the Platonic and Archimedean solids. For such types of particles, Torquato and Jiao [23,46] developed an optimization algorithm that they referred to as the adaptive shrinking cell (ASC) method, which is based on an MC method with the Metropolis acceptance rule. Except for tetrahedra, packings of other Platonic solids (cube, octahedra, dodecahedra, and icosahedra) generated by the ASC algorithm are their lattice packings. Since a cube is the only Platonic object that tiles the space, its lattice packing generated by the ASC algorithm is of densities close to unity and is highly ordered [23,46]. Indeed, in their paper, Torquato and Jiao state

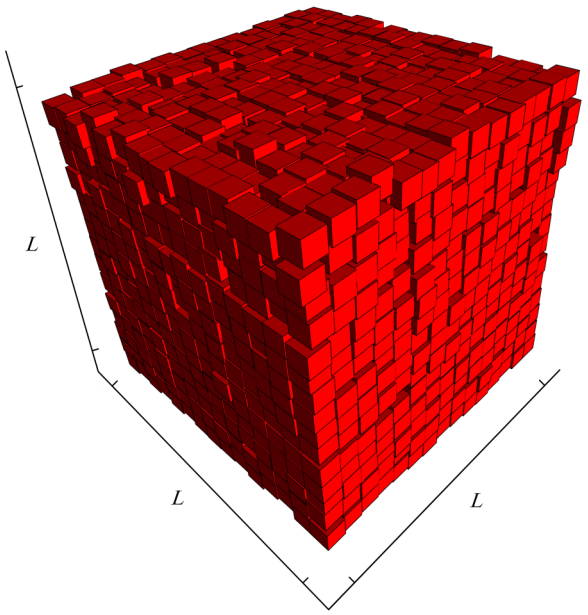

FIG. 2. Packing of nonoverlapping equal-sized cubic particles generated by the ASC algorithm. The packing fraction is 0.97.

[46] that, "We note that MRJ [maximally random jammed] packings of cubes were not studied here *because such packings produced via our ASC algorithm generally possess a very high degree of order due to the cubic symmetry of the solid and its ability to fill all of the space* (emphasis ours). This could be a deficiency of our ASC algorithm or any known hard-particle-packing algorithm in not being able to generate MRJ cube packings, or it is possible that the MRJ packings of hard cubes are intrinsically highly ordered. These issues will be examined in future work." An example is shown in Fig. 2.

Another algorithm for generating packings of cubic particles is the dynamic particle expansion (DPE) technique proposed by Delaney and Cleary [47]. The algorithm was originally developed for the so-called superellipsoids, defined by

$$\left(\frac{x}{a}\right)^m + \left(\frac{y}{b}\right)^m + \left(\frac{z}{c}\right)^m = 1, \tag{1}$$

where m is referred to as the shape parameter, and a, b, and c are the semimajor axes lengths. As m increases, the particles take on shapes that approach, for large values m, cubiclike. The DPE method utilizes a fully dynamic linear spring discrete-element method [48] to describe the interactions between the particles and a constant rate γ for their volumetric growth, and it is related to the algorithm developed by Lubachevsky and Stillinger [20] for hard particles. However, as Delaney and Cleary [47] note, "For superellipsoids with larger values of m (increasingly cubic shapes), we also observe an increase in Φ [the particle fraction in the model] as γ is reduced. However, the system forms *substantially denser packings at low growth rates and these packings exhibit clear signs of ordering, with highly ordered arrangements observed for large values of m*" (emphasis ours). Indeed, although cubiclike particles are generated, the overlap potential function introduced by Delaney and Cleary cannot generate packings of cubes with sharp vertices and nonsmooth edges.

We reported recently our preliminary results of a computer simulation of random packing of cubic particles of equal size and its microstructural characterization [49]. Since our goal is not generating highly ordered packings, we used neither the ASC algorithm of Torquato and Jiao [23,46] nor the DPE technique of Delaney and Cleary [47]. Therefore, we developed a version of the RSA algorithm to generate random packings of nonoverlapping monodisperse cubic particles. As long as one can introduce a nonoverlapping constraint for the particles, the RSA algorithm can be used to generate their random packings. Note, however, that the RSA algorithm is a computationally intensive method that results in a nonequilibrium system (frozen state), and it cannot be used to study the kinetics of a particle system.

The maximum packing fraction that we computed by our RSA algorithm was $\simeq$0.57, which represents the boundary between a liquid-crystal phase and a crystalline structure. This was consistent with the previously reported packing fractions for the random packings of cubic particles [24,50]. Furthermore, a variety of microstructural descriptors of the packings were reported, such as the radial distribution function, the face-normal correlation, and the two-point probability functions, along with the specific surface and mean chord length of the packings. In addition, we studied the effect of the porosity and finite system size on the characteristics, demonstrating that the packings possess both spatial and orientational long-range order at high packing fractions. In the present paper, we report further results for several other important microstructural descriptors of such packings, namely the two-point probability and cluster functions, the lineal-path and the pore-size distribution, as well as the surface-surface and surface void correlation functions. The correlation functions are, of course, among the key characteristics of any particle system.

The RSA algorithm that we have developed [49] begins with a large, empty region of volume V in $\mathbb{R}^3$, it generates cubic particles with randomly selected centers and orientations, and it places them sequentially in the volume. The deposition is subject to the nonoverlapping constraint, so that no newly inserted particle may overlap with any existing one. The addition process may be stopped at any time or step. The computational details of the RSA algorithm to generate random packings of nonoverlapping cubic particles are as follows, where we assume that all the cubic particles have the same size with the length of their edge being d_0.

Step 1. Specify the total number of cubic particles, N, and the cubes' length d_0, along with the size of the simulation cell, $L_x \times L_y \times L_z$.

Step 2. Generate three random numbers $x_c \in (0, L_x)$, $y_c \in (0, L_y)$, and $z_c \in (0, L_z)$ for the center of a new cubic particle.

Step 3. Generate two random numbers $u \in [-1, 1]$ and $\phi \in [0, 2\pi)$ for the normal vector $\mathbf{n}$ of the upper face of the cubes, expressed by

$$\mathbf{n} = \sqrt{1-u^2}\cos\phi\,\mathbf{i} + \sqrt{1-u^2}\sin\phi\,\mathbf{j} + u\,\mathbf{k}, \tag{2}$$

where $\mathbf{i}$, $\mathbf{j}$, and $\mathbf{k}$ are the three unit vectors in Cartesian coordinates (x, y, z).

Step 4. Determine the matrix $\mathbf{R}$ that rotates the unit vector $\mathbf{k}$ into the unit vector $\mathbf{n}$ through

$$\mathbf{R} = \mathbf{I} + \mathbf{A} + \mathbf{A}^2 \frac{(1-\mathbf{k})\cdot\mathbf{n}}{\|\mathbf{v}\|^2}, \tag{3}$$

where $\mathbf{I}$ is the identity matrix, and the unit vector $\mathbf{v} = (v_1, v_2, v_3)$ is defined by $\mathbf{k} \times \mathbf{n}$. Furthermore,

$$\mathbf{A} = \begin{bmatrix} 0 & -v_3 & v_2 \\ v_3 & 0 & -v_1 \\ -v_2 & v_1 & 0 \end{bmatrix}. \tag{4}$$

Note that if $\mathbf{n} = \mathbf{k}$, then $\mathbf{R} = \mathbf{I}$, and if $\mathbf{n} = -\mathbf{k}$, we have $\mathbf{R} = -\mathbf{I}$.

Step 5. The coordinates of the cube's eight vertices, $\mathbf{V}_i$, $i = [1,2,\ldots,8]$, are computed by

$$\mathbf{V}_i = \mathbf{V}_{\mathbf{i},\mathbf{n}} + \mathbf{V}_\mathbf{c}, \tag{5}$$

where $\mathbf{V}_c$ is the coordinate vector of the cube's center, and $\mathbf{V}_{i,n} = \mathbf{R}\mathbf{W}_i$, in which $\mathbf{W}_1 = (-d_0/2, -d_0/2, -d_0/2), \ldots, \mathbf{W}_8 = (d_0/2, d_0/2, d_0/2)$.

Step 6. Check to see if all the cube's vertices are outside the previously inserted particles. If so, accept the particle, and increase $n \to n+1$, where n is the current number of accepted particles. If $n \leqslant N$, go to step 2, or else terminate the simulation if the number of particles in the packing has reached its target.

It should be noted that the nonoverlapping constraint (NOC) in step 6 may be replaced by any other constraint. Various NOCs result, however, in diverse packing configurations and microstructural properties. For example, one may define the NOC as the distance between a new cube's vertices and those of the previously inserted particles' centers that must be greater than or equal to $d_0\sqrt{3}/2$. Such a constraint results in a smaller packing density than the aforementioned constraint.

III. MICROSTRUCTURAL DESCRIPTORS

To characterize the packings of cubic particles, the following microstructural descriptors and characteristic functions have been computed. We refer to the pore space and the solid particles as phases 1 and 2, respectively. Thus, the structure of the random packings depends on the packing density ϕ_2 or, equivalently, the porosity $\phi_1 = 1 - \phi_2$.

A. Two-particle probability density function

The most basic statistical descriptor for statistically homogeneous and isotropic systems of N particles is the two-particle probability density function $\rho(r)$, which is related to the radial distribution function $g(r)$ by

$$\rho(r) = \rho_2 g(r), \tag{6}$$

where ρ_2 is the number density of the particles, and $g(r)r^2dr$ is proportional to the conditional probability that a particle's centroid is in a spherical shell of thickness dr at a radial distance r from another particle's centroid at the origin. If there is no long-range order in the system, $\rho(r) \to \rho_2$, and thus $g(r)$ decays to unity very rapidly. For crystalline and quasicrystalline materials, however, in which remote portions of the same sample exhibit correlated behavior, $g(r)$ contains pronounced fluctuations around unity. Furthermore, it can be shown that

$$\int_0^\infty \rho(r)\Omega(d)r^{d-1}dr = N - 1, \tag{7}$$

where $\Omega(d) = 2\pi^{d/2}/\Gamma(d/2)$ is the volume of the d-dimensional spherical coordinate system, and it is equal to 4π for $d = 3$. Equation (7) implies that integrating $\rho_2 g(r)$ over the volume of a finite system yields the number of all the particles, except the one at the origin.

The contact number Z, defined as the mean number of the nearest neighbors of a given particle, is given by

$$Z = \int_{r_0}^{r_m} \rho(r)\Omega(d)r^{d-1}dr, \tag{8}$$

where r_0 is the rightmost position starting from $r = 0$ at which $\rho(r) = 0$, and r_m is the position of the first minimum after the first peak.

B. Face-normal correlation function

An important statistical descriptor for packings of nonspherical particles is the face-normal correlation function $C_{\mathrm{FN}}(\mathrm{r})$, defined as the average of the largest negative value of the inner product of two face normals of a pair of cubes p and q, separated by a distance r:

$$C_{\mathrm{FN}}(r) = \overline{\min(\mathbf{n}_{p,1,\ldots,6} \cdot \mathbf{n}_{q,1,\ldots,6})}. \tag{9}$$

The face-normal correlation function measures the extent to which a cube's orientation affects the orientation of another cube at a different position.

C. Two-point probability function

The two-point probability function $S_2^{(i)}(\mathbf{x}_1, \mathbf{x}_2)$ for phase i of a multiphase system, defined as

$$S_2^{(i)}(\mathbf{x}_1, \mathbf{x}_2) = \langle I^{(i)}(\mathbf{x}_1) I^{(i)}(\mathbf{x}_2) \rangle, \tag{10}$$

is one of the most important statistical descriptors of disordered media, representing the probability of finding two randomly selected points $\mathbf{x}_1$ and $\mathbf{x}_2$ in phase i, separated by a distance r. The indicator function is $I^{(i)}(\mathbf{x}) = 1$ if $\mathbf{x}$ belongs to phase i, and it is zero otherwise. For statistically homogeneous and isotropic media, $S_2^{(i)}(\mathbf{x}_1, \mathbf{x}_2)$ depends only on the distance r,

$$S_2^{(i)}(\mathbf{x}_1, \mathbf{x}_2) = S_2^{(i)}(r). \tag{11}$$

One also has $S_2^{(i)}(0) = \phi_i$, where ϕ_i is the volume fraction of phase i. In addition, $S_2^{(i)}$ must satisfy $\lim_{r\to\infty} S_2^{(i)}(r) \to \phi_i^2$. In particular, for two-phase disordered media, one has

$$S_2^{(2)}(r) = S_2^{(1)}(r) - 2\phi_1 + 1. \tag{12}$$

Note that there are certain relations between $S_2^{(i)}$ and other microstructural descriptors [6,8], so that any knowledge of $S_2^{(i)}$ leads directly to information about such descriptors.

D. Two-point cluster function

The *two-point cluster function* $C_2(\mathbf{x}_1, \mathbf{x}_2)$, defined as the probability of finding two points at $\mathbf{x}_1$ and $\mathbf{x}_2$ in the same cluster of phase i, is important to the macroscopic properties of the

packing. It is the analog of the two-point probability function $S_2^{(2)}(r)$ for the particle phase, but it contains connectedness information at the fine scale. Hence, its computation follows that of $S_2^{(2)}(r)$, except that only those events belonging to the same cluster must be counted. The two-point cluster function has been used in the reconstruction of disordered materials [51,52].

The *mean cluster size* S, defined as the average number of particles in the same cluster containing a randomly selected occupied particle, is also computed from the two-point cluster function via

$$S = \frac{\rho_2}{\phi_2^2}\int_0^\infty C_2(r)\Omega(d)r^{d-1}dr. \tag{13}$$

E. Lineal-path function

Another useful statistical descriptor of random packing of solid objects, which has also been utilized in the reconstruction of heterogeneous materials, is the lineal-path function $L^{(i)}(z)$, the probability of finding a randomly thrown line segment of length z entirely in phase i. Since $L^{(i)}(z)$ indicates connectedness along a lineal path of length z in phase i, it is also known as the coarse-scale connectedness function. The limiting values of the lineal-path function are $L^{(i)}(0) = \phi_i$ and $L^{(i)}(\infty) = 0$.

F. Chord-length distribution function

Chords are line segments between intersections of an infinitely long line with the two-phase interface. The cord-length probability density function $p^{(i)}(z)$ is defined for statistically isotropic media, such that $p^{(i)}(z)dz$ is the probability of finding a chord with a length between z and $z + dz$ in phase i. One of the most important factors affecting flow and transport properties of porous media is the mean chord length [3,53], defined by

$$l_C^{(i)} = \int_0^\infty z p^{(i)}(z)dz. \tag{14}$$

It can be shown that for any statistically isotropic system of arbitrary geometry, the chord-length distribution function is related to the lineal-path function according to

$$p^{(i)}(z) = \frac{l_C^{(i)}}{\phi_i}\frac{d^2L^{(i)}(z)}{dz^2}. \tag{15}$$

Furthermore, it is straightforward to show that for such systems, the mean chord length $l_C^{(i)}$ is related to the slope of the two-point probability function $S_2^{(i)}$ at the origin via

$$l_C^{(i)} = \frac{\phi_i}{-dS_2^{(i)}/dr\big|_{r=0}}. \tag{16}$$

G. Pore-size distribution function

The pore-size distribution function $P(\delta)$ for a porous medium is defined such that $P(\delta)d\delta$ is the probability that a randomly chosen point in the pore phase lies at a distance between δ and $\delta + d\delta$ from the nearest point on the pore-solid interface. Note that $P(\delta)$ is not the same as the classical pore-size distribution that is used to quantify the statistical distribution of the effective sizes of the pore bodies and pore throats of a pore space, and it is measured using a variety of techniques [3]. Since $P(\delta)$ is a probability density function, it normalizes to unity.

The associated cumulative distribution function $F(\delta)$ is the fraction of the pore space that has a pore radius larger than δ:

$$F(\delta) = \int_\delta^\infty P(r)dr. \tag{17}$$

Hence, its limiting values are $F(0) = 1$ and $F(\infty) = 0$.

H. Surface correlation functions

Surface correlation functions contain valuable information about the interface between the solid and pore phases, and they are of high importance in flow and transport properties of porous media [3,6,8]. As the one-point surface correlation function, the specific surface $s(\mathbf{x})$, defined as the interfacial area per unit volume, is proportional to the probability that $\mathbf{x}$ lies in a dilated space around the particles by a differential amount δd_0. In fact, the probability of finding a point in the dilated region around the particles in a homogeneous and isotropic packing is given by $s\delta d_0$. Moreover, another way of computing the specific surface s for d-dimensional isotropic porous media is based on using the first derivative of the two-point probability function $S_2^{(i)}$ with respect to r,

$$s = -\frac{\omega_d d}{\omega_{d-1}}\frac{dS_2^{(i)}}{dr}\bigg|_{r=0}, \tag{18}$$

where $\omega_d = \pi^{d/2}/\Gamma(1 + d/2)$ is the volume of a d-dimensional sphere of unit radius. After angular averaging, Eq. (18) is applicable to anisotropic media as well. Using the two-point probability function $S_2^{(i)}$ of each of the pore and solid phases in Eq. (18) leads to the same results for the specific surface.

Two-point surface correlation functions, namely the surface-surface correlation function $F_{ss}(\mathbf{x}_1,\mathbf{x}_2)$ and the surface-void correlation function $F_{sv}(\mathbf{x}_1,\mathbf{x}_2)$, have important roles in rigorous bounds on various flow and transport parameters, such as trapping constant and fluid permeability [6,8]. $F_{ss}(\mathbf{x}_1,\mathbf{x}_2)\delta d_0\delta d_0$ is defined as the probability that $\mathbf{x}_1$ and $\mathbf{x}_2$ both lie in a dilated space δd_0 around the particles. Furthermore, the probability that $\mathbf{x}_1$ lies in the dilated region and $\mathbf{x}_2$ lies in the void region (pore phase) is given by $F_{sv}(\mathbf{x}_1,\mathbf{x}_2)\delta d_0$. For statistically homogeneous and isotropic media, the two probabilities depend only on the distance r, and they take on the asymptotic forms $F_{ss}(r) \to s^2$ and $F_{sv}(r) \to s\phi_1$.

IV. RESULTS AND DISCUSSION

The densest random packing of cubic particles that we could generate by the RSA algorithm has a particle volume fraction of $\phi_2 \simeq 0.57$. Figure 3 presents an example of such a packing of cubic particles of size $d_0 = 0.05L$ and packing density of $\phi_2 = 0.3$, in a simulation cell of size $L \times L \times L$. The packing structure is homogeneous and isotropic.

Before presenting our results, let us first discuss the most important aspects of microstructural characterization of the packings reported previously [49]. We found [49] for the radial

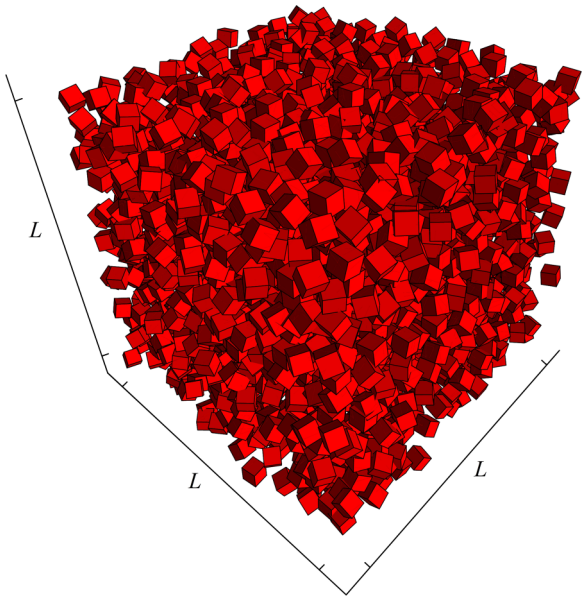

FIG. 3. Packing of nonoverlapping equal-sized cubic particles with $N = 2600$ and $d_0 = 0.05L$, where N is the number of particles. The packing density is $\phi_2 = 0.3$.

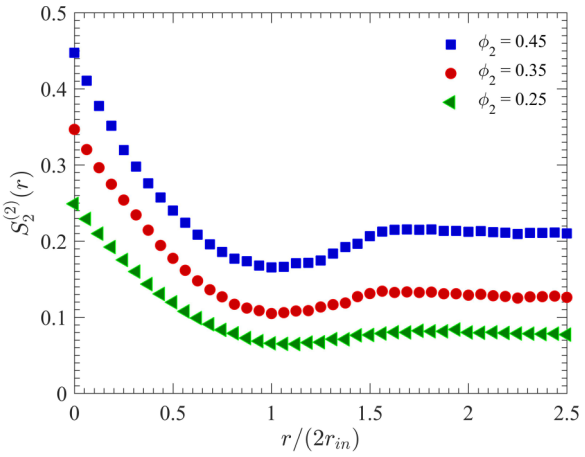

FIG. 4. Dependence on the packing density ϕ_2 of the two-point probability function $S_2(r)$ for the solid phase. r_{in} is the radius of the cubes' insphere.

distribution function $g(r)$, which describes how the density of a system varies as a function of the distance r, that although for all packing densities the first peak of $g(r)$ appears at $r \approx 1.4d_0$, its magnitude varies from 4.8 for $\phi_2 = 0.45$ to 3.6 for $\phi_2 = 0.35$ and 2.4 for $\phi_2 = 0.25$. Furthermore, the contact number Z, Eq. (8), turned out, respectively, to be $Z = 4.31$, 3.46, and 2.4 for the same particle fractions. In addition, the fluctuations of $g(r)$ beyond the first peak indicated long-range order in the system. We deduced that the denser packings exhibit better spatial long-range order, and that the crystallinity of the packing is better at higher packing fractions.

All the results that are presented here represent averages over at least 10 different realizations for each packing. The standard deviation of the results was at most 2% of the averages. The computed face-normal correlation function $C_{\text{FN}}(r)$ indicated that orientational long-range order is present in the system, and that the particles have many face-to-face contacts, and hence the largest angle between two normals to their faces is π. Therefore, C_{FN} is approximately 1, and the approximation is more accurate when the packing density is higher. The computed two-point probability function $S_2^{(1)}(r)$ for the pore phase of the same packings satisfied the theoretical prediction, $\lim_{r\to\infty} S_2^{(1)}(r) = \phi_1^2$. For porosities $\phi_1 \approx 0.55$, 0.65, and 0.75 and large radial distances r, we obtained $S_2^{(1)}(r) \approx 0.31$, 0.43, and 0.57, respectively.

The probability function $S_2^{(2)}$ for the solid phase of the packings, i.e., the pore space of the porous materials fabricated by the method described in the Introduction, is presented in Fig. 4, in which r_{in} is the cube insphere radius, i.e., $r_{\text{in}} = d_0/2$. The results are for packing densities, $\phi_2 = 0.45$, 0.35 and 0.25, and they are in excellent agreements with Eq. (11). In addition, for large distances r, $S_2^{(2)}(r)$ approaches 0.2, 0.13, and 0.07, respectively, hence satisfying the relation $\lim_{r\to\infty} S_2^{(2)}(r) = \phi_2^2$. The minima of the functions occur at a radial distance equal to the particle size, i.e., $r = 2r_{\text{in}} = d_0$. Moreover, with increasing pore sizes, $S_2^{(2)}(r)$ is a weak function of the distance, since the pore space has been enlarged, and therefore the probability that two points separated by a distance r are both in the solid phase becomes more or less independent of r.

Figure 5 presents the two-point cluster function $C_2(r)$ for the three packings of Fig. 4. As already mentioned, $C_2(r)$ contains useful information about the size of the clusters of the particles in a random packing, and it has been used in the reconstruction of models of random media. For short distances, $C_2(r)$ is an almost linear function of r in the interval $[0, r_{\text{in}}]$, but it approaches zero as $r \approx 1.2r_{\text{in}}$. As Eq. (13) indicates, since for higher packing densities ϕ_2 the area under the $C_2(r)$ curve is greater, the cluster sizes are also larger.

The lineal-path function $L^{(1)}(z)$ is the probability of finding a randomly thrown line segment of length z entirely in the pore phase. At $z = 0$, the function represents the porosity of the packing ϕ_1, and its tail, as it approaches zero, yields information about the largest possible line segment in the

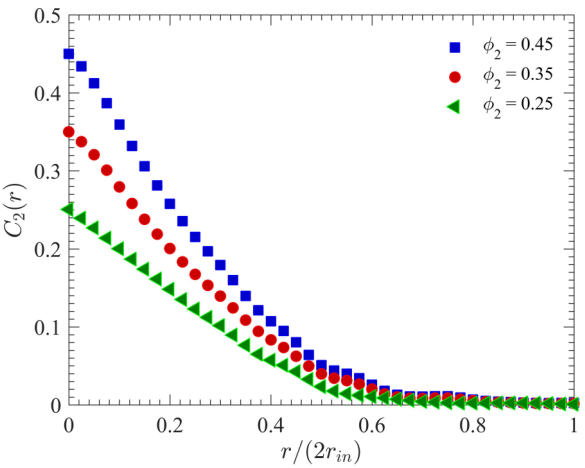

FIG. 5. Dependence on the packing density ϕ_2 of the two-point cluster function $C_2(r)$. r_{in} is the radius of the cubes' insphere.

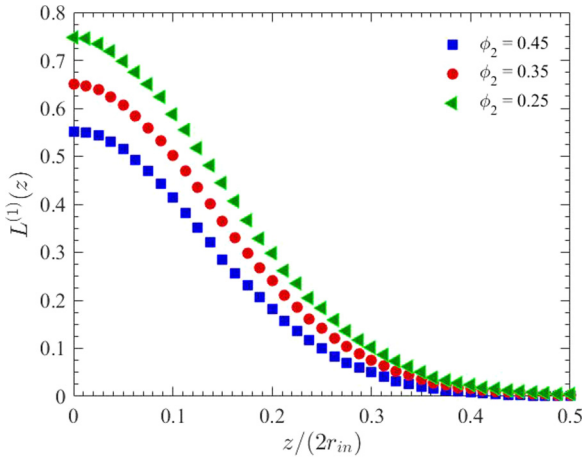

FIG. 6. Dependence on the packing density ϕ_2 of the lineal-path function $L(z)$ for the pore phase of the packing. r_{in} is the radius of the cubes' insphere.

pore space of the packing. Figure 6 shows the function for three packing densities. As expected, the largest possible line segment that is entirely in the pore space is larger for the looser packings. The maximum possible length of a line segment in this phase is around $0.5d_0$, which should be compared with the results for the solid phase, $L^{(2)}(z)$, presented in Fig. 7. As illustrated, the largest line segment z in the solid phase is less than the edge length of each cubic particle. Moreover, due to the nonoverlapping constraint, the tail is almost the same for all the packing densities.

The specific surface s and mean cord length l_C were already computed for the pore phase of the same packings and presented elsewhere [49]. They are important to fluid flow and transport through the pore space. Here, we report the results of the two characteristics for the solid phase of the packing, which could be useful to conduction and other transport processes through that phase, as well as to fluid flow and transport in the pore space of the porous media as the fabrication method described in the Introduction.

TABLE I. Dependence on the packing density ϕ_2 of the specific surface s and mean chord length $l_C^{(2)}$ of the solid phase.

	$\phi_2 = 0.45$	$\phi_2 = 0.35$	$\phi_2 = 0.25$
$s\ (L^{-1})$	46.86	34.11	25.28
$l_C\ (L)$	3.81×10^{-2}	4.06×10^{-2}	3.93×10^{-2}

Table I presents the two quantities for the three packings of Fig. 4. For fixed particle sizes, the denser the packings is, the larger is the specific surface. However, the pore space of the same packings also has smaller chord lengths. The computed results may be approximated by $s(\phi_2) \approx 107.87\phi_2 - 2.34$ and $l_C^{(2)}(\phi_2) \approx 0.04$. While the specific surface is independent of the pore and solid phases, i.e., the results are the same for both the pore and solid phases, the mean chord length in the solid phase of the packing is almost constant and smaller than the particle size ($d_0 = 0.05L$). This is once again due to the nonoverlapping constraint imposed on the packing.

Figure 8 illustrates the cumulative pore-size distribution function $F(\delta)$ for the three packings. As shown, $F(0)$ equals unity for all the packing densities. The tail of $F(\delta)$ at which it vanishes depends, however, on the packing fraction. In particular, for the denser packings, $F(\delta)$ is smaller than that of the looser ones. While $F(\delta)$ vanishes at $\delta \approx 0.3d_0$ for $\phi_2 = 0.45$, it does so at $\delta \approx 0.4d_0$ and $0.6d_0$ for $\phi_2 = 0.35$ and 0.25, respectively. This implies that no fraction of the pore space has a pore radius greater than $\delta \approx 0.3d_0$, $0.4d_0$, and $0.6d_0$, respectively, for the three packing fractions.

The surface-surface correlation function $F_{\text{ss}}(r)$, which is proportional to the probability of finding two end points of a line r that are both in the dilated region around the cubic particles, contains useful information about the internal surface of the porous media, and it has the dimensions of the inverse surface area. Figure 9 shows the two-body contribution to the surface-surface correlation function $F_{\text{ss}}(r)$ for three packing densities, scaled by the large-distance asymptotic value s^2. The two-body contribution to $F_{\text{ss}}(r)$ refers to the state in which points 1 and 2 are located on the surfaces of two different cubes.

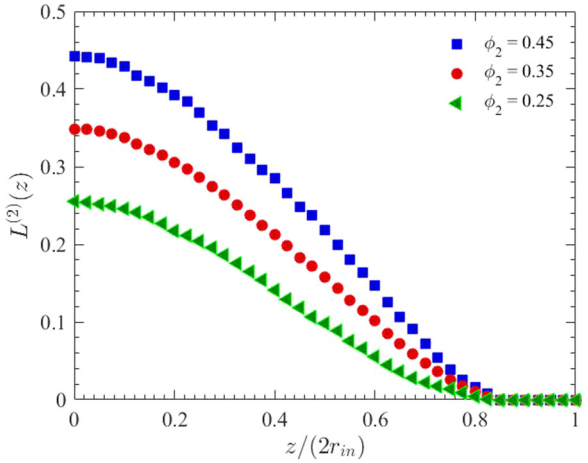

FIG. 7. Dependence on the packing density ϕ_2 of the lineal-path function $L(z)$ for the solid phase of the packing. r_{in} is the radius of the cubes' insphere.

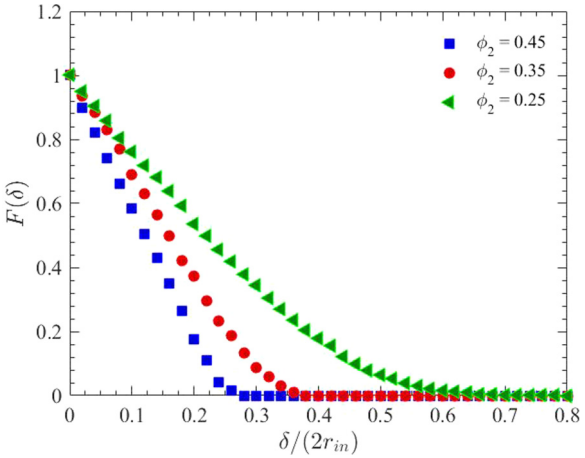

FIG. 8. Dependence on the packing density ϕ_2 of the cumulative pore-size distribution function $F(\delta)$. r_{in} is the radius of the cubes' insphere.

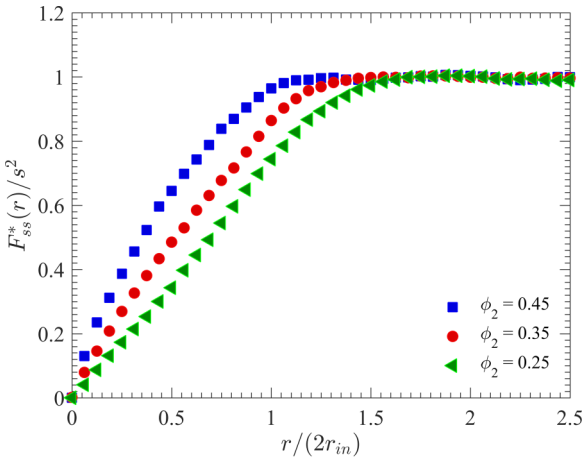

FIG. 9. Dependence on the packing density ϕ_2 of the scaled two-body contribution to the surface-surface correlation function $F_{ss}(r)$. r_{in} is the radius of the cubes' insphere.

Theoretically, since $\lim_{r\to\infty} F_{ss}(r)$ is equal to the square of the specific surface s, one has $F_{ss}(r)/s^2 \to 1$ for large radial distances r. As illustrated, the values of $F_{ss}(r)$ are greater and their approach to unity is faster for higher packing densities. In particular, $F_{ss}(r)$ approaches s^2 at $r \approx d_0$ for $\phi_2 = 0.45$, implying that at distances greater than $\approx d_0$, the surface-surface correlation function is the square of the internal surface-to-volume ratio.

The surface-void correlation function $F_{sv}(r)$ is the probability of finding one end point of a line r in the pore space and the other one in the dilated region around the particles. Figure 10 presents the scaled two-body contribution to the surface-void correlation function $F_{sv}(r)/(s\phi_1)$ for the same three packing densities as before. In a manner similar to the surface-surface correlation function, $F_{sv}(r)/(s\phi_1) \to 1$ for large distances r, which Fig. 10 confirms. In addition, Fig. 10 indicates that values of $F_{sv}(r)$ are greater and their approach to unity is sharper for higher packing densities. Both $F_{ss}(r)$ and $F_{sv}(r)$ have many applications in determining the fluid permeability and bounds for the reactive trapping constant of porous media [6,8].

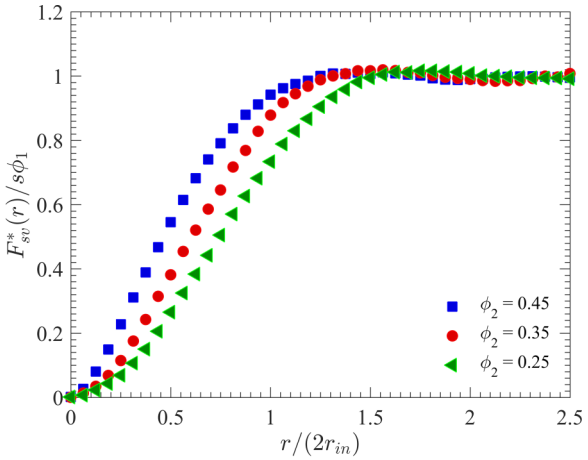

FIG. 10. Dependence on the packing density ϕ_2 of the scaled two-body contribution to the surface-void correlation function $F_{sv}(r)$. r_{in} is the radius of the cubes' insphere.

V. SUMMARY

This paper presented the results of a detailed simulation of the microstructural descriptors for random packings of nonoverlapping and equal-size cubic particles. A version of the RSA algorithm was introduced to generate random packings, and some of the most important statistical descriptors were calculated and analyzed, including the two-point probability and cluster functions, the lineal-path and pore-size distribution functions, as well as the surface-surface and surface-void correlation functions. Furthermore, the specific surface and mean cord length were computed and analyzed for different packing fractions.

The random packings that we have studied possess both spatial and orientational long-range order. The results reveal that the denser packings have a structure similar to liquid crystals at a particle volume fraction of $\phi_2 \geqslant 0.45$. As long as the densest achievable packing is about $\phi_2 \approx 0.57$, the packings with fixed density but smaller particle sizes have larger specific surfaces (which is expected) but smaller chord lengths for the pore phase. This feature is the same for denser packings with fixed particle sizes.

While the microstructural descriptors for such packings have never been computed and analyzed before, the maximum particle volume fraction of random packings of hard cubes has been reported by Baker and Kudrolli [24] and Agarwal and Escobedo [50]. Hence, our computed maximum packing fraction may be compared with theirs. The maximum packing fractions reported previously [24,50] are 0.45 for the isotropic phase and 0.57 for the liquid-crystal state (the mesophase), hence agreeing with what we have computed. According to Agarwal and Escobedo [50], the maximum packing exhibits mesophase behavior. Hence, the upper limit for our random packings of hard cubes ($\phi_2 \simeq 0.57$) is a boundary between the liquid-crystal phase and crystalline structure.

Comparison of our results with those of dense packings of other Platonic solids [23,24], and in particular with packings of tetrahedral particles, indicates that random packings of cubic particles have better-structured configurations. In fact, although the radial distribution function for such packings exhibits behavior similar to our results but with a faster decay to unity, their orientational correlation function indicates face-to-face contacts between only neighboring particles, implying short-range orientational correlations. This is in contrast with the random packings studied here, which exhibit both spatial and orientational long-range order.

ACKNOWLEDGMENTS

M.S. acknowledges many useful discussions with his collaborators in Ref. [43], particularly A.R. Mehrabi, which provided part of the impetus for the present work. The initial stage of this work was supported by the Avery Dennison Corporation. Partial support of this work by the Petroleum Research Fund, administered by the American Chemical Society, is gratefully acknowledged.

[1] M. E. Davis, Ordered porous materials for emerging applications, Nature (London) **417**, 813 (2002).

[2] M. E. Davis and R. F. Lobo, Zeolite and molecular sieve synthesis, Chem. Mater. **4**, 756 (1992).

[3] M. Sahimi, *Flow and Transport in Porous Media and Fractured Rock*, 2nd ed. (Wiley-VCH, Weinheim, 2011).

[4] R. Zallen, *The Physics of Amorphous Solids* (Wiley, New York, 1983).

[5] P. M. Chaikin and T. C. Lubensky, *Principles of Condensed Matter Physics* (Cambridge University Press, New York, 2000).

[6] S. Torquato, *Random Heterogeneous Materials* (Springer, New York, 2002).

[7] S. F. Edwards, in *Granular Matter*, edited by A. Mehta (Springer-Verlag, New York, 1994).

[8] M. Sahimi, *Heterogeneous Materials I: Linear Transport and Optical Properties* (Springer, New York, 2003).

[9] M. Sahimi, *Heterogeneous Materials II: Nonlinear and Breakdown Properties and Atomistic Modeling* (Springer, New York, 2003).

[10] M. Shahinpoor, Statistical mechanical considerations on the random packing of granular materials, Powder Technol. **25**, 163 (1980).

[11] B. A. Cornell, J. Middlehurst, and N. S. Parker, Modeling the simplest form of order in biological membranes, J. Colloid Interface Sci. **81**, 280 (1981).

[12] T. I. Quickenden and G. K. Tan, Random packing in two dimensions and the structure of monolayers, J. Colloid Interface Sci. **48**, 382 (1974).

[13] W. B. Russel, D. A. Saville, and W. R. Schowalter, *Colloidal Dispersion* (Cambridge University Press, Cambridge, 1989).

[14] S. Torquato and A. K. Sen, Conductivity tensor of anisotropic composites from the microstructure, J. Appl. Phys. **67**, 1145 (1990).

[15] J. D. Sherwood, Packing of spheroids in three-dimensional space by random sequential addition, J. Phys. A **30**, L839 (1997).

[16] Y. T. Feng, K. Han, and D. R. J. Owen, An advancing front packing of polygons, ellipses, and spheres, in *Proceedings of the Third International Conference on Discrete Element Methods*, edited by B. J. Cook and R. P. Jensen (ASCE, Santa Fe, NM, 2002), p. 93.

[17] A. Donev, I. Cisse, D. Sachs, E. A. Variano, F. H. Stillinger, R. Connelly, S. Torquato, and P. M. Chaikin, Improving the density of jammed disordered packings using ellipsoids, Science **303**, 990 (2004).

[18] W. Man, A. Donev, F. H. Stillinger, M. T. Sullivan, W. B. Russel, D. Heeger, I. Inati, S. Torquato, and P. M. Chaikin, Experiments on Random Packings of Ellipsoids, Phys. Rev. Lett. **94**, 198001 (2005).

[19] F. M. Schaller, M. Neudecker, M. Saadatfar, G. W. Delaney, G. E. Schroder-Turk, and M. Schroter, Local Origin of Global Contact Numbers in Frictional Ellipsoid Packings, Phys. Rev. Lett. **114**, 158001 (2015).

[20] B. D. Lubachevsky and F. H. Stillinger, Geometric properties of random disk packings, J. Stat. Phys. **60**, 561 (1990).

[21] O. U. Uche, F. H. Stillinger, and S. Torquato, Concerning maximal packing arrangements of binary disk mixtures, Physica A **342**, 428 (2004).

[22] A. Donev, J. Burton, F. H. Stillinger, and S. Torquato, Tetratic order in the phase behavior of a hard-rectangle system, Phys. Rev. B **73**, 054109 (2006).

[23] S. Torquato and Y. Jiao, Dense packings of polyhedra: Platonic and Archimedean solids, Phys. Rev. E **80**, 041104 (2009).

[24] J. Baker and A. Kudrolli, Maximum and minimum stable random packings of platonic solids, Phys. Rev. E **82**, 061304 (2010).

[25] P. F. Damasceno, M. Engel, and S. C. Glotzer, Predictive self-assembly of polyhedra into complex structures, Science **337**, 453 (2012).

[26] E. R. Chen, D. Klotsa, M. Engel, P. F. Damasceno, and S. C. Glotzer, Complexity in Surfaces of Densest Packings for Families of Polyhedra, Phys. Rev. X **4**, 011024 (2014).

[27] J. H. Conway and S. Torquato, Packing, tiling, and covering with tetrahedra, Proc. Natl. Acad. Sci. (USA) **103**, 10612 (2006).

[28] A. Haji-Akbari, M. Engel, A. S. Keys, X. Zheng, R. G. Petscheke, P. Palffy-Muharay, and S. C. Glotzer, Disordered, quasicrystalline and crystalline phases of densely packed tetrahedra, Nature (London) **462**, 773 (2009).

[29] J.-P. Latham, Y. Lu, and A. Munjiza, A random method for simulating loose packs of angular particles using tetrahedrons, Geotechnique **51**, 871 (2001).

[30] A. Baule, R. Mari, L. Bo, L. Portal, and H. A. Makse, Mean-field theory of random close packings of axisymmetric particles, Nat. Commun. **4**, 2194 (2013).

[31] W. Jin, P. Lu, and S. Li, Evolution of the dense packings of spherotetrahedral particles: From ideal tetrahedra to spheres, Sci. Rep. **5**, 15640 (2015).

[32] B. Widom, Random sequential addition of hard spheres to a volume, J. Chem. Phys. **44**, 3888 (1966).

[33] J. Feder, Random sequential adsorption, J. Theor. Biol. **87**, 237 (1980).

[34] D. W. Cooper, Parking problem (sequential packing) simulations in two and three dimensions, J. Colloid Interface Sci. **119**, 442 (1987).

[35] O. Gromenko and V. Privman, Random sequential adsorption of oriented superdisks, Phys. Rev. E **79**, 042103 (2009).

[36] G. Zhang and S. Torquato, Precise algorithm to generate random sequential addition of hard hyperspheres at saturation, Phys. Rev. E **88**, 053312 (2013).

[37] S. Torquato, T. M. Truskett, and P. G. Debenedetti, Is Random Close Packing of Spheres Well Defined? Phys. Rev. Lett. **84**, 2064 (2000).

[38] A. Donev, S. Torquato, and F. H. Stillinger, Neighbor list collision-driven molecular dynamics for nonspherical hard particles: I. algorithmic details, J. Comput. Phys. **202**, 737 (2005).

[39] A. Donev, S. Torquato, and F. H. Stillinger, Neighbor list collision-driven molecular dynamics for nonspherical hard particles: II. applications to ellipses and ellipsoids, J. Comput. Phys. **202**, 765 (2005).

[40] W. S. Jodrey and E. M. Tory, Computer simulation of close random packing of equal spheres, Phys. Rev. A **32**, 2347 (1985).

[41] M. D. Rintoul and S. Torquato, Hard-sphere statistics along the metastable amorphous branch, Phys. Rev. E **58**, 532 (1998).

[42] S. Torquato and F. H. Stillinger, Jammed hard-particle packings: from Kepler to Bernal and beyond, Rev. Mod. Phys. **82**, 2633 (2010).

[43] A. R. Mehrabi, L. Vaziri, J. de Santos, R. Mehrabi, and M. Sahimi, Novel method for fabrication of porous materials with controlled morphology, Adv. Mater. (to be published).

[44] L. Rossi, S. Sacanna, W. T. M. Irvine, P. M. Chaikin, D. J. Pine, and A. P. Philipse, Cubic crystals from cubic colloids, Soft Matter **7**, 4139 (2011).

[45] M. Norouzi Rad, N. Shokri, and M. Sahimi, Pore-scale dynamics of salt precipitation in drying porous media, Phys. Rev. E **88**, 032404 (2013).

[46] Y. Jiao, and S. Torquato, Maximally random jammed packings of Platonic solids: Hyperuniform long-range correlations and isostaticity, Phys. Rev. E **84**, 041309 (2011).

[47] G. W. Delaney, and P. W. Cleary, The packing properties of superellipsoids, Europhys. Lett. **89**, 34002 (2010).

[48] *Discrete-Element Modeling of Granular Materials*, edited by F. Radjaï and F. Dubois (Wiley, Hoboken, NJ, 2011).

[49] H. Malmir, M. Sahimi, and M. R. Rahimi Tabar, Microstructural characterization of random packings of cubic particles, Sci. Rep. **6**, 35024 (2016).

[50] U. Agarwal, and F. A. Escobedo, Mesophase behavior of polyhedral particles, Nat. Mater. **10**, 230 (2011).

[51] Y. Jiao, F. H. Stillinger, and S. Torquato, A superior descriptor of random textures and its predictive capacity, Proc. Natl. Acad. Sci. (USA) **106**, 17634 (2009).

[52] C. E. Zachary and S. Torquato, Improved reconstructions of random media using dilation and erosion processes, Phys. Rev. E **84**, 056102 (2011).

[53] C. E. Krohn, and A. H. Thompson, Fractal sandstone pores: Automated measurements using scanning-electron-microscope images, Phys. Rev. B **33**, 6366 (1986).